Heating the air in buildings by evacuated tube solar collector used AL_2O_3/ water nanofluid at Cairo-Egypt climates

Abdalla Gomaa, Fifi N. M. Elwekeel, Mahmoud Abdelmagied, Momen I. Radwan

Refrigeration and Air-Conditioning Technology Dpt, Faculty of Industrial Education, Helwan University, 11282 Cairo, Egypt

Abstract

The present paper investigates experimentally the performance of the evacuated tube heat pipe solar collector in Cairo-Egypt climate conditions. The experimental work conducts by using an evacuated solar collector with nanofluid in indirect building heating. The investigation parameters are tilt angle, AL_2O_3 nanoparticles concentrations, mass flow rates, water temperature difference, useful heat gain, collector thermal efficiency, air temperature difference, thermal optical efficiency and energy loss coefficients. The results show that the tilt angle 45^o gives best performance characteristics of the collector. At tilt angle of 45^o, 90 kg/h flow rate, 0.2% of nanofluid concentration and at 1:30 PM the air temperature difference increases by 16.4% than the reference fluid. The collector thermal efficiency increases by high concentrations of nanofluid, which reaches to 49%, 44.8%, 42.9% and 39% at a nanofluid concentration of 0.2%, 0.15%, 0.1% and 0% at 1:30 PM and 90kg/h, respectively. Also at low mass flow rate the air temperature difference increases by 9^oC at 0.2% of nanofluid concentration.

Key words: evacuated tube; nanofluid; performance; solar collector; heating.

Nomenclature

A	Collector aperture area	[m^2]		**Subscripts**
Cp	Specific heat capacity	[J/kg/k]	*a*	absorbed
F_R	Heat removal factor	[-]	*amb*	ambient
I	Solar radiation intensity	[W/m^2]	*bf*	Base fluid
k	Thermal conductivity	[W/m.K]	*coll.*	Collector
$\dot{m}$	Mass flow rate of fluid	[kg/s]	*f*	Fluid
$\dot{Q}$	Heat energy	[W]	*i*	Inlet
T	Temperature	[W]	*o*	Outlet
U	Overall heat losses coefficient	[W]	*L*	Losses
Greek Letters		[^oC]	*hl*	Heat losses
τ	Transmittance	[-]	*nf*	Nanofluid
α	Absorptance	[-]	*np*	Nano-particles
η	Efficiency of collector	[%]	*rad*	Radiation
ρ	Density	[kg/m^3]	*u*	useful
φ	concentration of nano-particles	[-]		

Abbreviations

ETHPSC	Evacuated Tube Heat Pipe Solar Collector

1. Introduction

The energy consumption of heat pump system or electric heaters increases in a winter season. That makes the solar thermal systems is effective, sustainable and renewable for such cases, in addition to the fossil fuel problems. The main part of solar system is the solar collector because it receives the solar intensity and converts it to thermal energy. The efficiency of solar collector is important parameter, so there are more methods to enhance the thermal efficiency of solar collector. The recent method used nanofluids as a working fluid in the solar collectors.

Sharfeldin and Grof [1, 2] presented the performance of evacuated tube heat pipe solar collector using CeO_2/ water and WO_3/ water at different flow rates and concentrations. The study indicated that the thermal efficiency of the collector enhanced with increased nanofluids concentration. Also, the thermal optical efficiency of the collector was 34% and 72.8% for CeO_2/ water and WO_3/ water; respectively. Ayompe and Duffy [3] analyzed the performance of solar heating system with evacuated tube solar collector. The data recorded that the maximum outlet fluid temperature was 70.3^oC, the temperature at the lowest level of the

storage tank was 59.5^{o}C and the collector efficiency was 63.2%. Hyeongmin et al. [4] investigated experimentally the effects of the nanoparticle size and concentration of Al_2O_3 on U-tube solar collector; they found that the maximum efficiency reached 72.4% at nanoparticle size of 20 nm. Hussein et al. [5] taken nanofluid concentration of Ag and ZrO_2 mixed with distilled water as working fluid in evacuated tube collector. They found that the evacuated tube collector performed better using Ag nanofluid compared with ZrO_2 nanofluid. The effects of AL_2O_3/distilled water nanofluid on the performance of evacuated tube collector were investigated experimentally by Javad and Sidik [6]. The results showed that the collector efficiency was enhanced by increasing the concentration of AL_2O_3 nanofluids, the maximum collector efficiency was 57.63% with a concentration of 0.06% nanofluid (by volume). An experimental study was conducted to evaluate the performance of a thermosyphon heat pipe flat plate collector using AL_2O_3 – water nano fluid by Pise et al. [7]. They used various nanofluid concentrations of 0.05, 0.25 and 0.5 with five tilt angels. The results showed that AL_2O_3 – water gave high collector performance compared to water; the collector performance was recorded 15.24% at 0.5 wt% Water-Al_2O_3. Effects of AL_2O_3 nanofluid on the performance of the evacuated tube collector were investigated by Al-Mashat and Hasan [8] in Baghdad climate. The results showed that by increasing nanofluid concentration, the efficiency of the solar collector increased.

Putra et al. [9] studied the performance of evacuated tube heat pipe solar collector with 0.1% nanofluid concentration of Al_2O_3-water and at different inclination angles. The optimal tilt angle was 30^{o} according to Indonesia climate. Kang et al. [10] used CuO nanofluid and water as working fluid in evacuated tube solar collector, they showed that at concentration of 0.1 vol%, 0.3 vol% and 0.7 vol% the efficiency enhanced by 4.4 %, 2.3 % and 0.3 % ; respectively compared to water. Daghigh and Shafieian [11] conducted a theoretical and experimental evaluation of the performance of the heating system using evacuated tube heat pipe solar collector. According to analysis, the optimal number of collector tubes was 15 tubes and the maximum outlet temperature of the collector was 64^{o}C.

The performance of evacuated U-tube solar collector was investigated by Kaya et al. [12]. They used ZnO nano particles with ethylene glycol-pure water as working fluid, the maximum thermal efficiency of collector was determined by 62.87% at a concentration of 3% nanofluid and a flow rate of 0.045kg/s. An experimental and numerical study of the performance of U- tube evacuated tube collector was introduced by Kiran et al. [13]. They observed that the useful heat gained was influenced by solar intensity, mass flow rate and inlet temperature of working fluid while the ambient temperature had no effect on them.

Mustafa [14] presented a research on the effects of the different working fluids on the energetic and exergetic performance of thermosyphon evacuated tube solar collectors. They investigated hexane, petroleum ether, chloroform, acetone, methanol and ethanol as working fluids. By hexane the solar collector gave less energy and exergy efficiencies.

Jafarkazemi et al. [15] reported that the inlet water temperature, water flow rates, transmittance of tubes and absorptance had directly affected on the energetic and exergetic efficiencies of the evacuated tube heat pipe solar collector. Further Olcha et al. [16] investigated the energetic and exergetic efficiencies for evacuated tube solar collector using mixture of water and propylene glycol as working fluid. Based on the results the energy and exergy efficiencies reached 58.8% and 3.75%; respectively. An experimental study was carried out on the evacuated tube solar collector using graphene nanoplatelets (GNP)/distilled water by Iranmanesh et al. [17]. The enhanced thermal efficiency of the collector was 90.7% at a flow rate 1.5 L/min.

From above mentioned review, it can be seen there is no investigation studies conducted on evacuated solar collector using nanofluids at Cairo climate to investigate the performance of the collector. Also all studies use evacuated solar collector with nanofluid in heating water applications. So, the aims of present study are:

- Investigation of the thermal performance of evacuated solar collector using nanofluid at Cairo climate to determine the best tilt angle in winter season.
- Use evacuated solar collector with nanofluid to indirectly heat the air.

2. Test Methodology

2.1 Preparation method for Nonofluid

AL_2O_3 nano-particles have average diameter of 55 nm (Fig.1), which are checked with transmission electron microscopy (TEM). The distilled water is considered as a reference fluid. The preparation process is conducted by three steps. Firstly, the required weight of nano-particles is measured by a digital electronic balance. Secondary, distilled water -AL_2O_3 nano-particles are mixed by magnetic stirrer for two hours to obtain homogeneous mixture as shown in Fig.2. The last step is ultrasonification process, which is applied to the mixture for two hours to break up agglomeration and obtain a stable nanofluid by good distribution of nano-particles in the water (Fig.3). The physical properties of water and AL_2O_3 nano-particles are presented in Table 1.

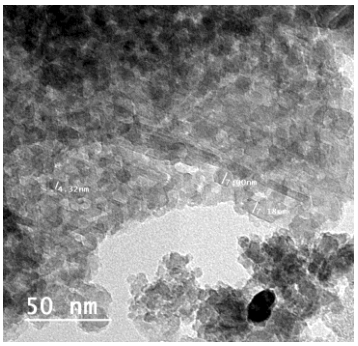

Fig. 1 photograph for AL_2O_3 Nano-particles by TEM apparatus

Fig. 2 AL_2O_3 magnetic stirring

Fig. 3 AL_2O_3 ultrasonification

Table (1) the physical properties of water and AL_2O_3 nano-particles.

Specification	ρ (kg/m^3)	C_p (J/kg.K)	K(W/m.K)	μ(pa.s)
water	999	4180	0.60	$1.003x10^{-3}$
AL_2O_3 nano-particles	3880	773	36	-

2.2 Experimental Set-up

Figure 4 shows the experimental set-up which consists of three loops. There are solar collector loop (Loop A), evacuated tube heat pipe collector ETHPSC with specific geometric characteristics indicated in Table 2. Heating coil loop (Loop B) and air side loop (Loop C). In Loop A, the working fluid heats in the ETHPSC and the first centrifugal pump is used to circulated the fluid between the ETHPSC and the storage tank, which has a capacity of 60 liters. The heated fluid flows from the storage tank to the fin and tube heating coil by a second centrifugal pump in the loop B. Finally, in the loop C air flows through the heat exchanger to get the heat from the heated fluid.

The experimental procedures are carried out through winter season according to Cairo – Egypt weather conditions with latitude 30.04^o N and longitude of 31.23^o E. The evacuated tube heat pipe solar collector ETHPSC is placed facing to south orientation and set up at various tilt angles of the collector of 15^o, 25^o, 35^{o}and 45^o. The flow rates of the working fluid are changed from 60 kg/hr to 150 kg/hr based on ASHRAE Standard [18]. Every run of the experiment are from 8:30 AM to 4:30 PM for the mostly clear sky days. Time interval for every run was 5 minutes.

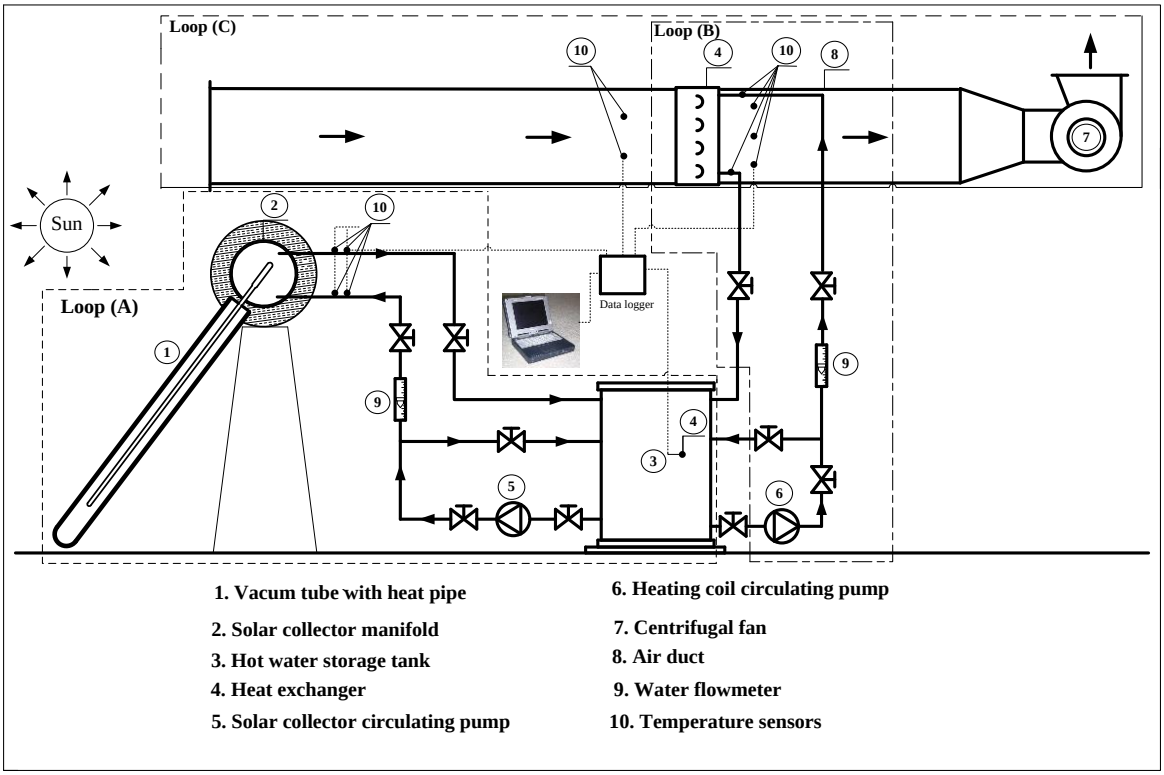

Fig. 1 Schematic diagram for the experimental test rig

Table (2) the geometric characteristic of the evacuated tube heat pipe collector

Specification	Dimensions/Material	Units
Collector Dimensions (LxW)	1.5 x 1.25	m^2
No. of evacuated tubes	15	--
Collector aperture area (A_c)	1.305	m^2
Glass material	Borosilicate glass	--
Glass tube outer / inner diameter	58/51	mm
Glass tube length	1500	mm
Glass transmittance	0.9	--
Glass Absorptance	0.93	--
Emission factor	0.08	--
Heat pipe evaporator diameter /length	6/1400	mm
Heat pipe condenser diameter /length	9/100	mm
Heat transfer fin material	Aluminum	--
Manifold material	Stainless Steel 304	--
Manifold diameter/ length	100/1250	mm

2.3. Measuring technique.

The temperatures are measured by 16 temperature sensors of LM-35 with an accuracy of ±0.4^{o}C across solar collector, heating coil, storage tank and ambient conditions.

The intensity of solar radiation is measured by solar radiation sensor with ±0.01 accuracy. All these sensors are connected by a data logger. Volume flow rates are measured by using floating flow meters with an accuracy of ±0.5 LPM. The air velocity profile through the duct section is identified according to ASHRAE recommendations [19]. The hot wire anemometer is used to obtain the average air velocity with an accuracy of ±0.1 m/s, which were 1 m/s and constant during all experiments. Also, the electrical data (volts and amperes) of pumps and fan motors are recorded.

2.4. Measurements uncertainties

The experimental error analysis indicates the effect of error of the measured parameters on the uncertainty of the results. The uncertainty analysis of the various parameters through the study is calculated according to Holman, [20]. Given W_1, W_2, W_3, ..., W_n uncertainties in the independent variables (X_1, X_2, X_3, ...X_n) and W_R is the uncertainty in the result at the same odds, then the uncertainty in the result can be given as;

$$W_R = \left[\left(\frac{\partial R}{\partial X_1} W_1 \right)^2 + \left(\frac{\partial R}{\partial X_2} W_2 \right)^2 + \left(\frac{\partial R}{\partial X_3} W_3 \right)^2 + ...+ \left(\frac{\partial R}{\partial X_n} W_n \right)^2 \right]^{\frac{1}{2}} \quad (1)$$

The maximum uncertainties in measuring and calculated parameters under investigation are given in the Table 3.

Table 3 Uncertainty of measured parameters

Instruments	unit	Uncertainty (%)
Temperature	^{o}C	±0.88
Solar radiation intensity	W/m^2	±0.012
Flow meter	L/min	±7.14
Air velocity anemometer	m/s	±0.08
Collector efficiency	-	±7.19

3. Data Reduction

Inlet temperature of the fluid ($T_{f,i}$), outlet temperature of the fluid ($T_{f,o}$), ambient temperature (T_{amb}) and solar radiation intensity (I_{rad}) are parameters that have effects on the performance of the evacuated tube heat pipe solar collector ETHPSC . The difference between absorbed heat ($\dot{Q}_a$) and heat losses $\dot{Q}_{h.l}$ is a useful heat gain rate, which is absorbed from the solar collector and can be expressed as follows,

$$\dot{Q}_u = \dot{Q}_a - \dot{Q}_{h.l} = \dot{m}_f Cp_f \left(T_{f,o} - T_{f,i}\right) \quad (2)$$

Another expression of the useful heat gain rate can be calculated by Fabio [21] as:

$$\dot{Q}_u = F_R . A_{coll.} \left[I_{rad} (\tau\alpha) - U_L \left(T_{f,i} - T_{amb}\right)\right] \quad (3)$$

Where U_L is the overall heat losses coefficient

The instantaneous efficiency of the solar collector is given by [22]:

$$\eta_{coll.} = \frac{\dot{m}_f Cp_f \left(T_{f,o} - T_{f,i}\right)}{I_{rad} . A_{coll.}} = \frac{F_R . A_{coll.} \left[I_{rad} (\tau\alpha) - U_L \left(T_{f,i} - T_{amb}\right)\right]}{I_{rad} . A_{coll.}} \quad (4)$$

$$= F_R \left(\tau\alpha\right) - F_R . U_L \left(\frac{T_{f,i} - T_{amb}}{I_{rad}} \right) \quad (5)$$

Eq. (5) known as Hottel – Whillier equation

Then the heat removal factor can be given by:

$$F_R = \frac{\dot{m}_f Cp_f \left(T_{f,o} - T_{f,i}\right)}{A_{coll.} \left[I_{rad} (\tau\alpha) - U_L \left(T_{f,i} - T_{amb}\right)\right]} \quad (6)$$

The physical properties of nanofluid which is density (ρ), specific heat capacity (C_p), thermal conductivity (k) and dynamic viscosity (μ) are calculated as the following equations:

$$\rho_{nf} = \rho_{np} \left(\varphi\right) + \rho_{bf} \left(1 - \varphi\right) \quad (7)$$

$$Cp_{nf} = \frac{(\rho Cp)_{np}(\varphi) + (\rho Cp)_{bf}(1-\varphi)}{(\varphi)\rho_{np} + \rho_{bf}(1-\varphi)} \quad (8)$$

$$k_{nf} = k_{bf}(1 + 8.733\varphi) \quad (9)$$

$$\mu_{nf} = \mu_{bf} . \exp\left(\frac{(5.989\varphi)}{(0.278-\varphi)}\right) \quad (10)$$

Where φ is the volume concentration of nanofluid /water

4. Results and Discussions:

In this paper the effect of tilt angles of the collector, working fluid mass flow rates and water nanofluid concentrations on the performance characteristics of evacuated tube heat pipe collector and heat gained for air are investigated as the following:

4.1 Effects of tilt angles of the collector:

The effects of tilt angles of the collector on performance characteristics of ETHPSC are presented in this section. The inclination angles are 15^o, 25^o, 35^o and 45^o using distilled water as a working fluid.

Fig. 5 shows the intensity of solar radiation during daylight hours. It can be seen that the intensity of solar radiation increases with the daylight hours until it reaches to a peak in the afternoon and falls down at the rest of the daytime. It is also clear that the increase in the tilt angles of the collector increases the receiving solar radiation so; the optimum angle is 45^o according to Cairo latitude. The maximum intensities of solar radiation are 940 W/m^2, 900 W/m^2, 880 W/m^2 and 800 W/m^2 for 45^o, 35^o, 25^o and 15^o; respectively at 1:30 PM.

The water temperature difference across ETHPSC during daylight hours is presented in Fig.6. Clearely the water temperature difference has the same trend of intensity of solar radiation. The highest values of water temperature difference are made by 45^o tilt angle. The water temperature difference reaches to 4.6^{o}C at 1:30 PM and 45^o tilt angle.

Fig. 7 illustrates the variation of useful heat gain from ETHPSC with daylight hours at different tilt angles of the collector and flow rate of 90 kg/hr. This figure selected as example to show the effects of tilt angles on useful energy gained from this collector. The useful heat gain is increased from morning until it reaches maximum values in the afternoon, which are 480 W, 429 W, 379 W and 308 W for tilt angles 45^o, 35^o, 25^o and 15^o; respectively. By 45^o tilt angle the highest useful energy gained can be achieved, this is due to the high water temperature difference (Eq.2).

The relation among thermal efficiency of ETHPSC and tilt angles is shown in Fig. 8. Higher thermal efficiency is recorded at 45^o tilt angle and the maximum thermal efficiency value occurs at 1:30 PM. Obviously, the water temperature difference.

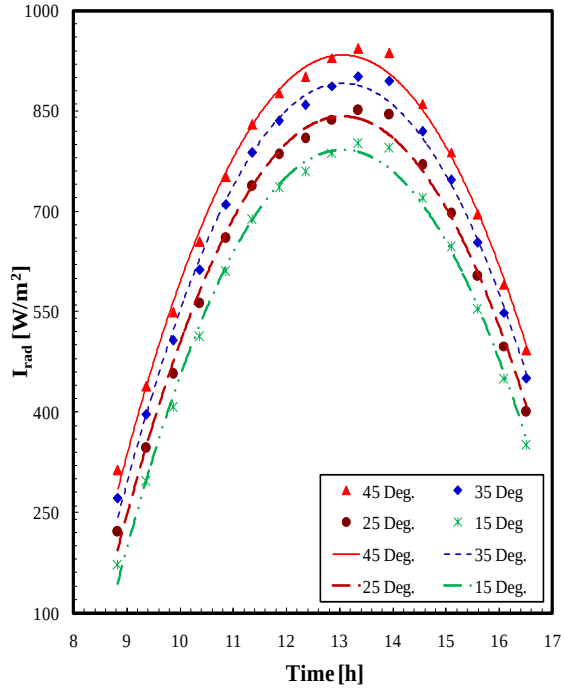

Fig. 5 Solar radiation versus time at different tilt angles

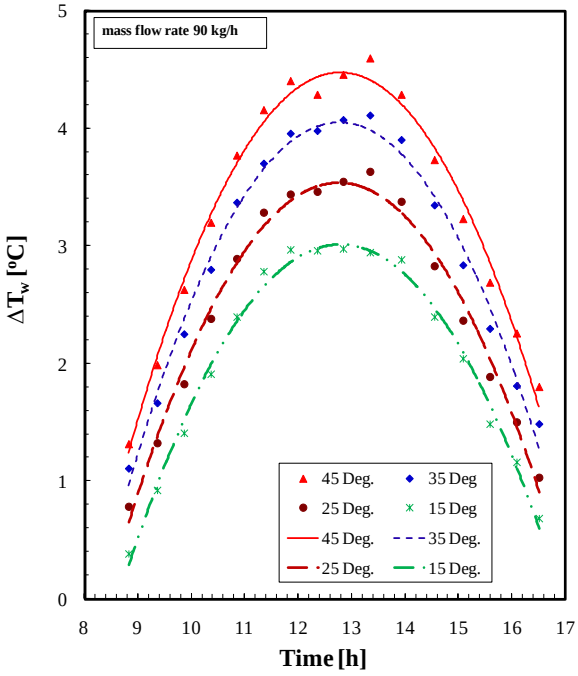

Fig.6 Water temperature difference across ETHPSC with different tilt angles

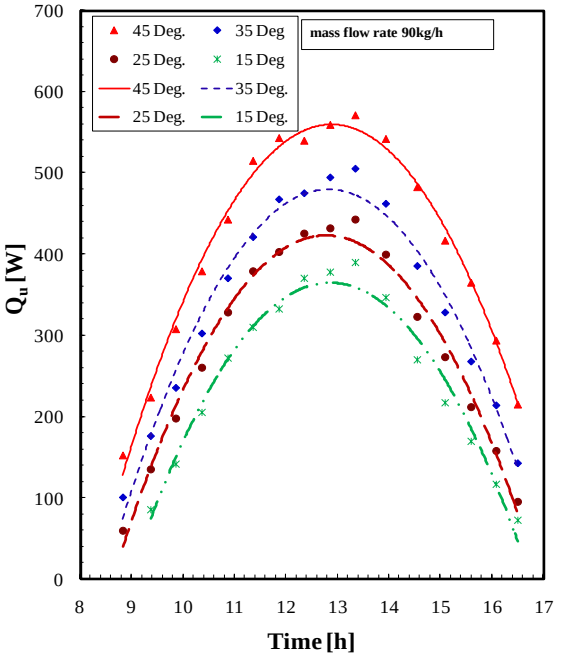

Fig. 7 Useful energy gain for different tilt angles

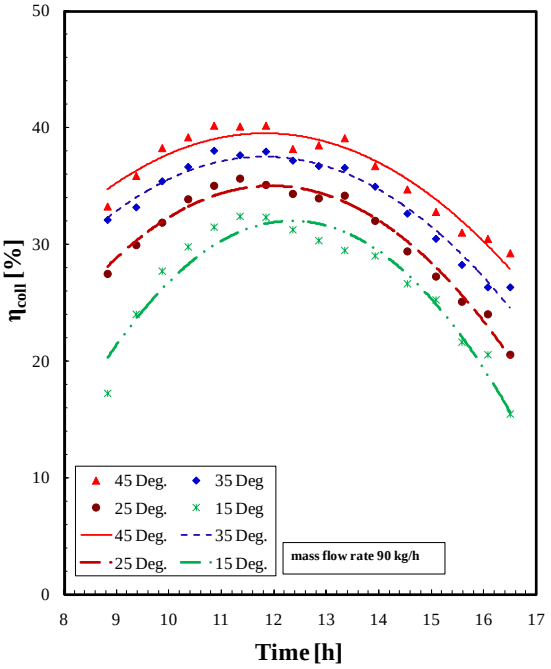

Fig.8 Efficiency of ETHPSC for different tilt angles

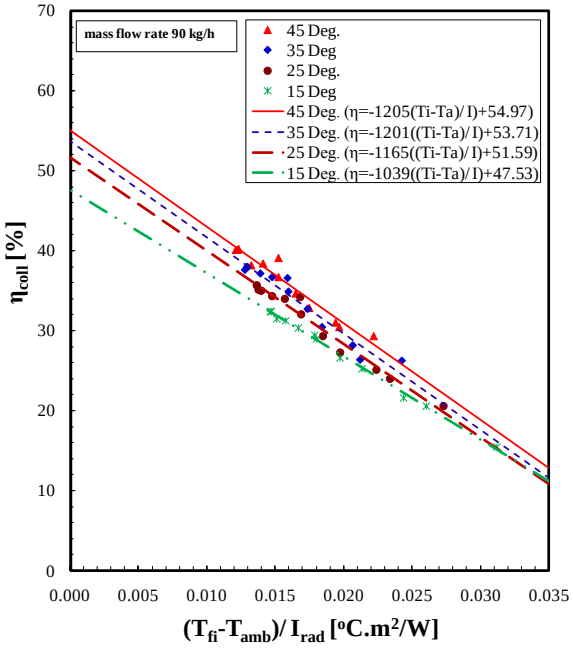

Fig.9 Relation between collector efficiency, $(T_i-T_a)/I$ and tilt angles

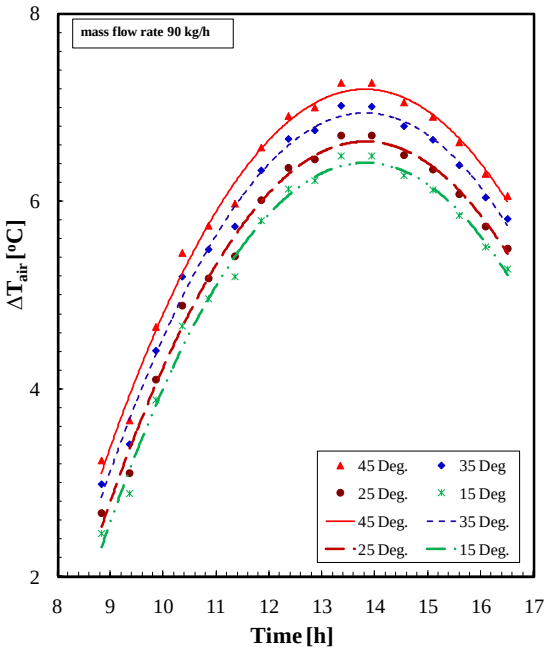

Fig.10 Air temperature difference across heat exchanger

Table (4) $F_R(\tau\alpha)$ and $(-F_R .U_L)$ parameters at different tilt angles and mass flow rates.

Mass flow rate (kg/hr)	Tilt angle	$F_R(\tau\alpha)$	$-F_R .U_L$ (W/m^2.K)	R^2
60 kg/hr	15°	0.434	10.10	0.949
	25°	0.443	10.34	0.945
	35°	0.460	11.16	0.943
	45°	0.477	11.24	0.960
90 kg/hr	15°	0.468	10.39	0.996
	25°	0.512	11.65	0.969
	35°	0.520	12.01	0.942
	45°	0.544	12.05	0.944
120 kg/hr	15°	0.569	10.90	0.920
	25°	0.602	11.74	0.967
	35°	0.619	12.16	0.968
	45°	0.652	12.48	0.942
150 kg/hr	15°	0.634	11.45	0.965
	25°	0.660	11.91	0.946
	35°	0.677	12.30	0.956
	45°	0.686	13.05	0.965

has a significant effect on the thermal efficiency than solar radiation intensity. At 1:30 PM, the thermal efficiency of 45° is increased by 6.4%, 12.4% and 24.5% compared to 35°, 25° and 15°; respectively

Fig. 9 illustrates the relation among collector efficiency and [(Ti-Ta)/I] parameter at different tilt angels. The collector efficiency is decreased with increasing [(Ti-

Ta)/I]. The intersection point with Y-axis is known as the thermal optical efficiency FR(τα) or it is called the energy absorbed by the collector. According to ASHRAE [18], the slope of this linear curve determines the coefficient of energy loss from the collector (-FR.UL).

Fig.10 shows the relation between air side temperature difference, tilt angles and daylight hours. The difference in air temperature increases as daylight hours increase until 1:30 PM and after 1:30 PM the curve falls. This corresponds to water temperature trends (see Fig. 6). At tilt angle of 45^o and at 1:30 PM the air temperature increases by 7.2^oC.

Table (4) shows the values of $F_R(\tau\alpha)$, $(-F_R .U_L)$ and root mean square for different tilt angles of the collector and flow rates. It is clear that the 45^o tilt angle gives higher values of the thermal optical efficiency at different mass flow rates 45^o tilt angle has the highest energy loss coefficients, but by 45^o tilt angle, the collector receives high solar radiation intensity which is enhanced the thermal efficiency of the collector as Fig.8. 45^o tilt angle has the highest energy loss coefficients, but by 45^o tilt angle, the collector receives high solar radiation intensity which is enhanced the thermal efficiency of the collector as Fig.8.

From Figs.7-10 and table (4), the tilt angle 45^o has better thermal performance characteristics for ETHPSC depending on the Cairo location. So it will be chosen as tilt angle in the rest results.

6.2 Effect of AL_2O_3/water nanofluid

As the previous section, the highest performance characteristics of ETHPSC are achieved at a 45^o tilt angle. Therefore, the experimental work is carried out at a 45^o tilt angle, mass flow rate of 90kg/hr and at varying concentrations of AL_2O_3/water. The volume concentrations of nanofluid are 0%, 0.1%, 0.15% and 0.2%.

Fig. 11 illustrates the effects of nanofluid on working fluid temperature variation through ETHPSC during daylight hours. It is obvious that the difference in the working fluid temperature is enhanced by the addition of nanofluid. Because the thermal conductivity increases with increasing of nanofluid concentration due to random fluctuation (Brownian movement) of particles as result of forced circulation of the fluid and consequently increases heat transfer coefficient. The highest working fluid temperature difference can be done at a concentration of 0.2%, which is increased by 16% than reference fluid (0%) at 1:30 PM.

Useful heat gain of ETHPSC with varying nanofluid concentrations at 90 kg/hr is indicated in Fig.12. The thermal gain rate of ETHPSC increases with the concentrations of nanofluid due to the improvement of physical properties of the working fluid. At 1:30 PM a useful heat gain are increased than that of reference fluid (0%) by about 16.5%, 10.8% and 7.3% at concentrations of 0.2%, 0.15% and 0.1%, respectively.

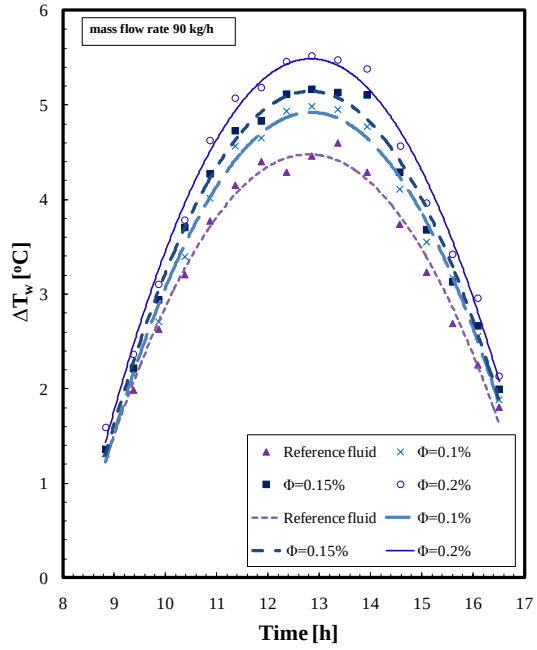

Fig. 11 working fluid temperature difference with varying concentration of nanofluid

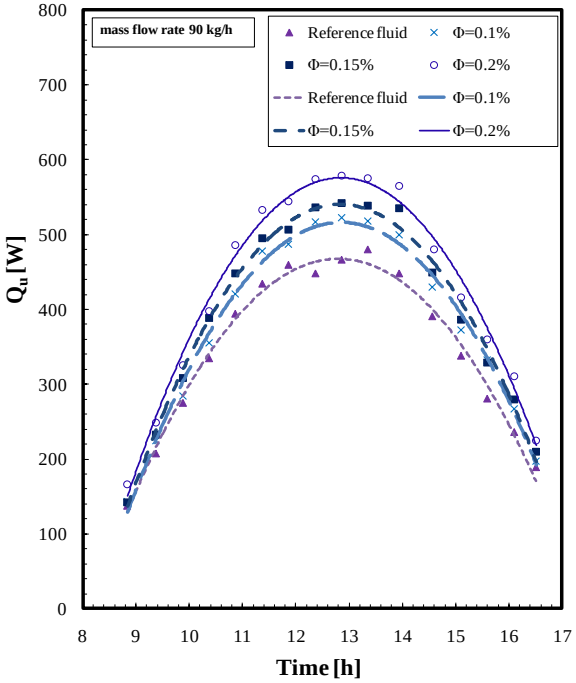

Fig.12 useful heat gain versus with time for different nanofluid concentration

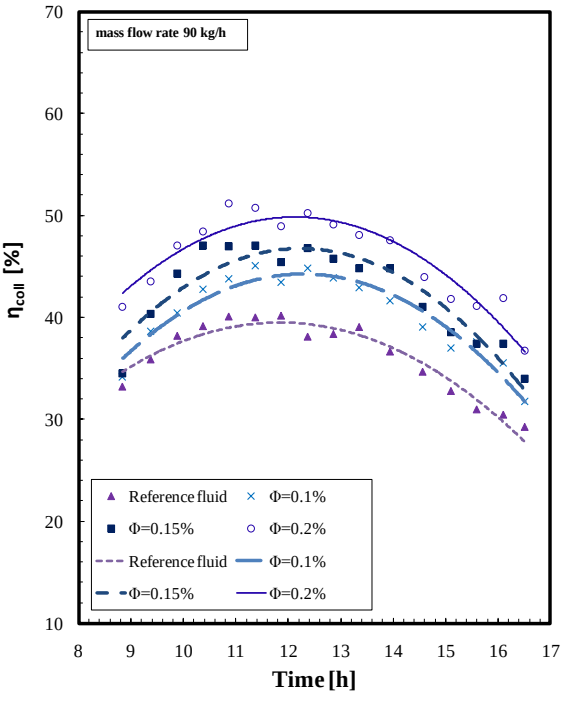

Fig.13 efficiency of ETHPSC for different water nanofluid
concentration and mass flow rate 90 kg/hr

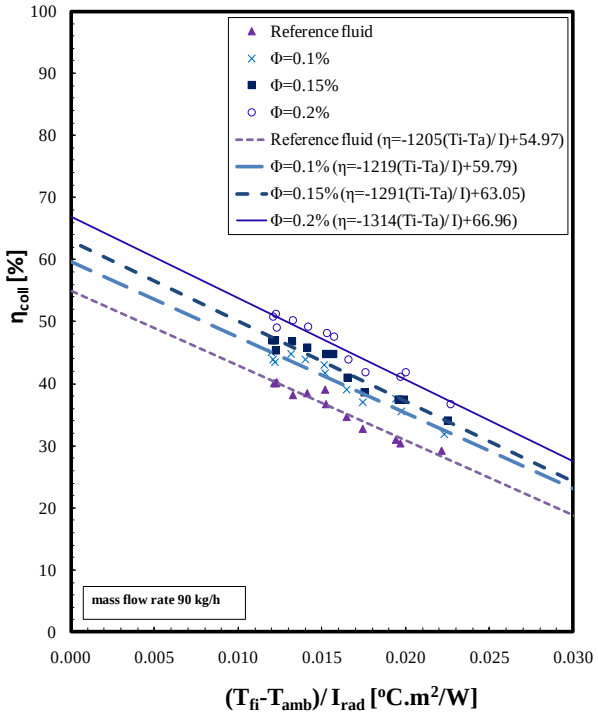

Fig. 14 Efficiency of ETHPSC with [(Ti-Ta)/I] at different concentrations of nanofluid

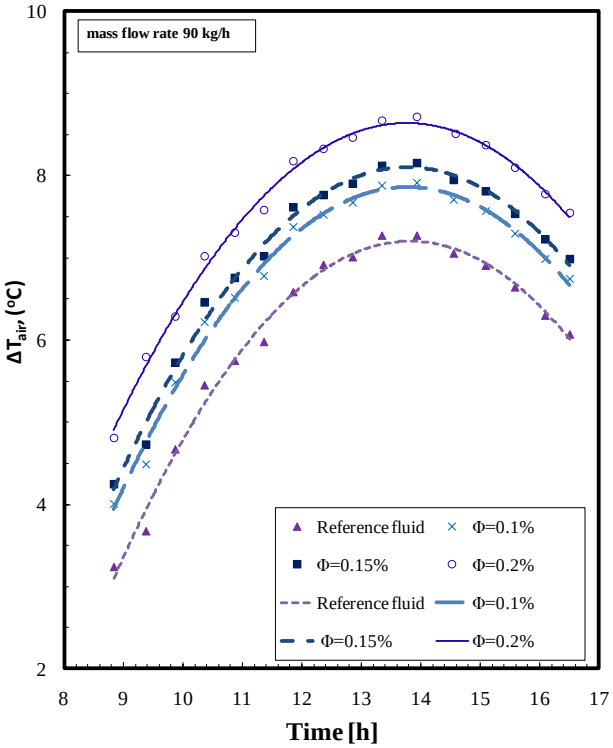

Fig.15 variation of air side temperature difference through heat exchanger

Fig.13 presents the relation between the thermal efficiency, daylight hours and concentrations of nanofluid. The change in useful heat gain has a significant effect on thermal efficiency of ETHPSC as shown in this figure. It can be seen that the thermal efficiency at concentrations of 0.2%, 0.15%, 0.1% and 0% reaches to 49%, 44.8%, 42.9% and 39% at 1:30 PM, respectively.

The relation between thermal efficiency of ETHPSC, $[(T_i-T_a)/I]$, thermal optical efficiency and energy losses coefficient are presented in Fig.14. The thermal efficiency of ETHPSC decreases with increasing $[(T_i-T_a)/I]$ while the thermal efficiency of ETHPSC is increased with increasing concentrations of nanofluid. At concentrations of 0.2%, 0.15% and 0.1%, the thermal optical efficiency $FR(\tau\alpha)$ of ETHPSC is greater than the reference fluid by about 18.2%, 13.5% and 8.4%; respectively. The energy loss coefficient $(-F_R.U_L)$ is increased by 8.3%, 6.7% and 1.2% compared with reference fluid at 0.2%, 0.15% and 0.1% nanofluid concentrations.

Fig.15 shows the effects of nanofluid concentration on air side temperature during daylight hours. Obviously, the air temperature difference has high values through high concentrations of nanofluid because the heat transfer characteristics of the working fluid are enhanced by the addition of nanoparticles. By nanofluid concentrations of 0.2%, 0.15% and 0.1%, the air temperature difference is higher than the reference fluid by about 16.4%, 10.3% and 7.8%; respectively, at 1:30 pm.

6.3 Effect of mass flow rate

The mass flow rates are important parameter in the solar collectors design, so in this section, the effect of mass flow rate of reference fluid and 0.2% nanofluid concentrations will be investigated at 45^o tilt angle.

Fig.16 shows the relation between water temperature difference through collector with daylight times for reference fluid and AL_2O_3/ water mixture at a concentration of 0.2% at different mass flow rates of 60 kg/h, 90 kg/h, 120 kg/h and 150 kg/h.

For two cases the water temperature difference is increased with lower mass flow rates, the highest water temperature difference can be obtained at a flow rate 60 kg/h.

At the same inlet water temperature with decreasing of flow rate, the working fluid has a low velocity which helped it to get more heat and therefore produce higher temperature difference. At the same condition with 0.2% of nanofluid concentration, the water temperature difference is higher than that the reference fluid by 22.6% at a flow rate of 60 kg/h and 1:30 PM.

Fig. 17 presents a useful energy gain with a flow rate of working fluid over daylight times. The useful energy gain has high values with increasing the flow rate. Because the useful energy gain is a function of water temperature difference and mass flow rate so, the mass flow rate has a higher effect on the increase of useful energy than the difference in water temperature. Also by 0.2% of nanofluid concentration the useful energy gain is enhanced at different mass flow rates. At 1:30 PM and 0.2% of nanofluid concentration, the useful energy gain at 60kg/h, 90kg/h, 120 kg/h and 150kg/h are higher than the reference fluid by about 22.9%, 16.5% and 8.3%; respectively. Fig. 18 shows the trend of the collector thermal efficiency with daylight times at 45^o tilt angle, 0.2% of nanofluid concentration and different flow rates of working fluid. The trend of collector thermal efficiency is depended on useful energy gain. So the maximum collector thermal efficiency is achieved at mass flow rate of 150 kg/h. The collector thermal efficiency is higher than reference fluid by about 6.7% at mass flow rate of 150 kg/h and a 0.2%.of nanofluid concentration.

Thermal optical efficiency $F_R(\tau\alpha)$ and energy losses coefficient $(-F_R.U_L)$ as a function of mass flow rate are shown in Fig. 19. Both have higher values at high mass flow rate and with nanofluid concentration. At concentration of nanofluid of 0.2%, the thermal optical efficiency are increased compared with reference fluid by about 10.2%, 8.8%, 18% and 23% at mass flow rates of 150 kg/h, 120 kg/h, 90 kg/h and 60 kg/h, respectively.

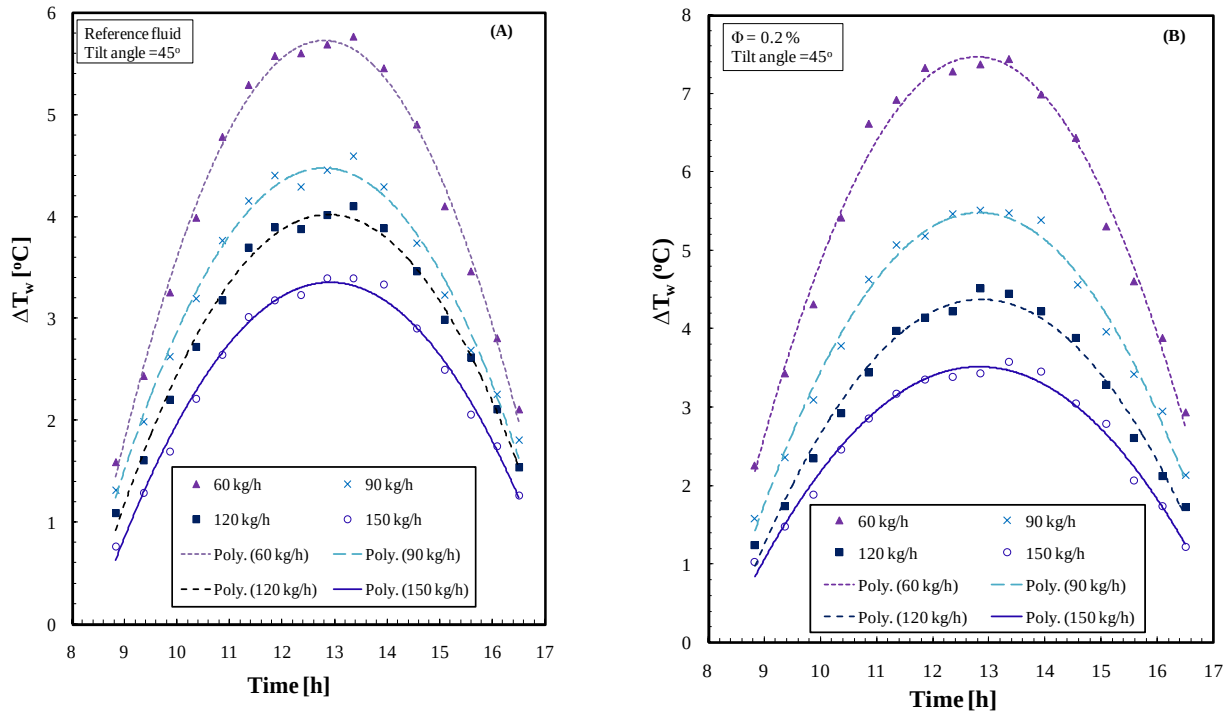

Fig.(16) water temperature difference through collector vs time for base water at different mass flow rates**,[A]** Reference fluid, **[B]**working fluid with 0.2% nanofluid concentration

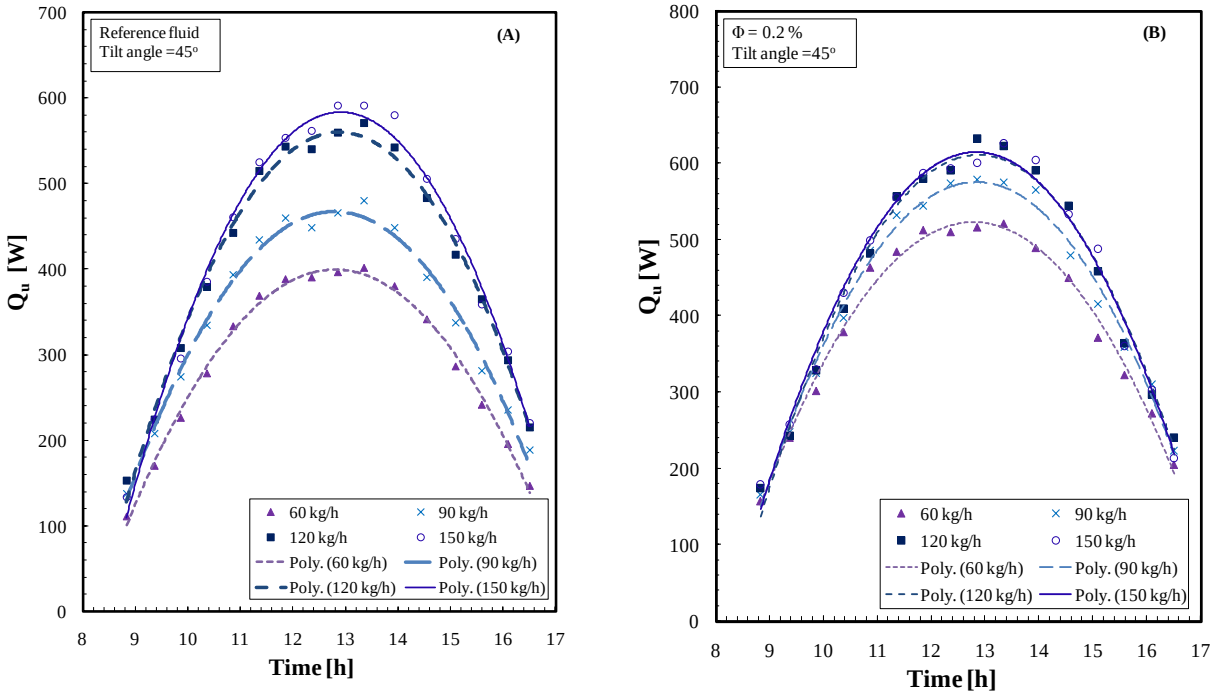

Fig.(17) Useful energy gained by collector vs time for base water at different mass flow rates

,**[A]** Reference fluid, **[B]**working fluid with 0.2% nanofluid concentration

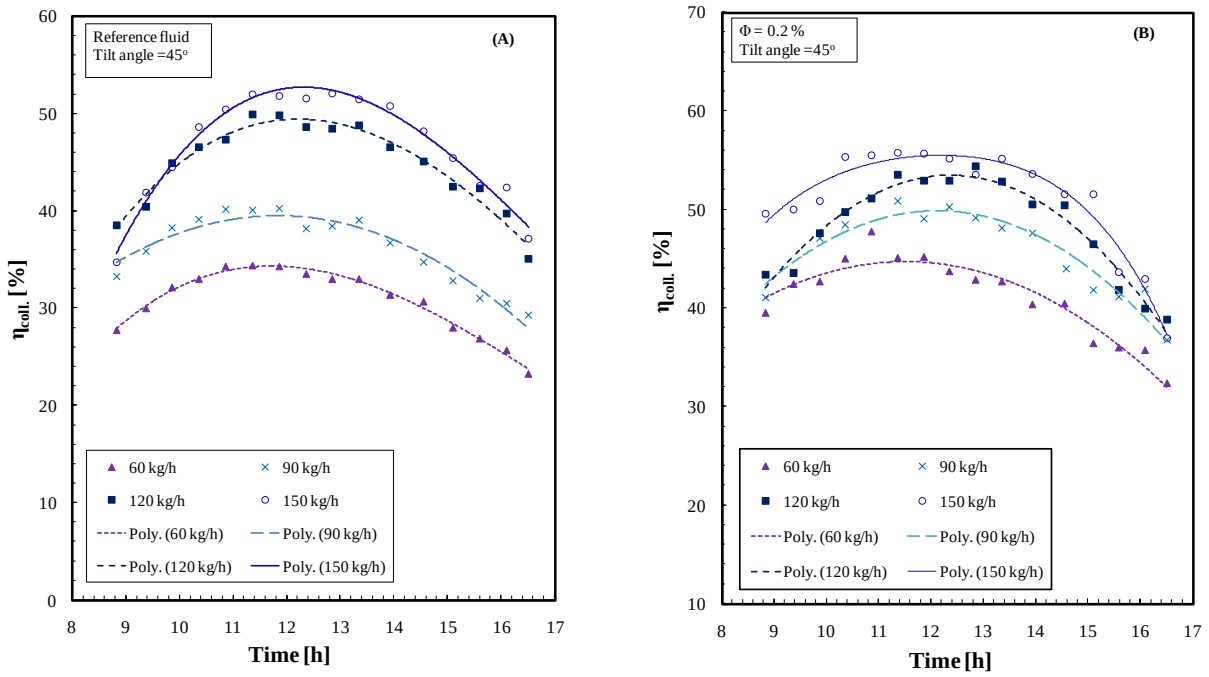

Fig.(18) Thermal efficiency of solar collector vs time for base water at different mass flow rates

,[A] Reference fluid, **[B]**working fluid with 0.2% nanofluid concentration

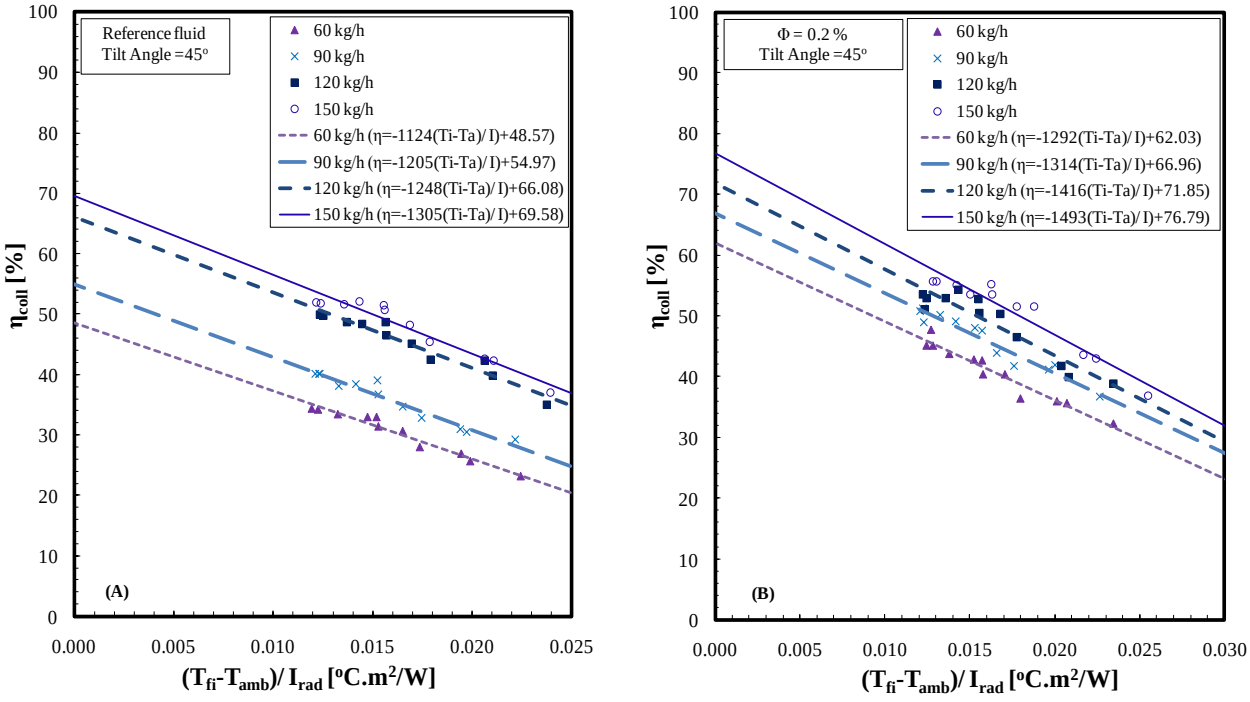

Fig.(19) Relation between thermal efficiency of ETHPSC, mass flow rates and $[(T_i-T_a)/I]$, **,[A]** Reference fluid, **[B]**working fluid with 0.2% nanofluid concentration

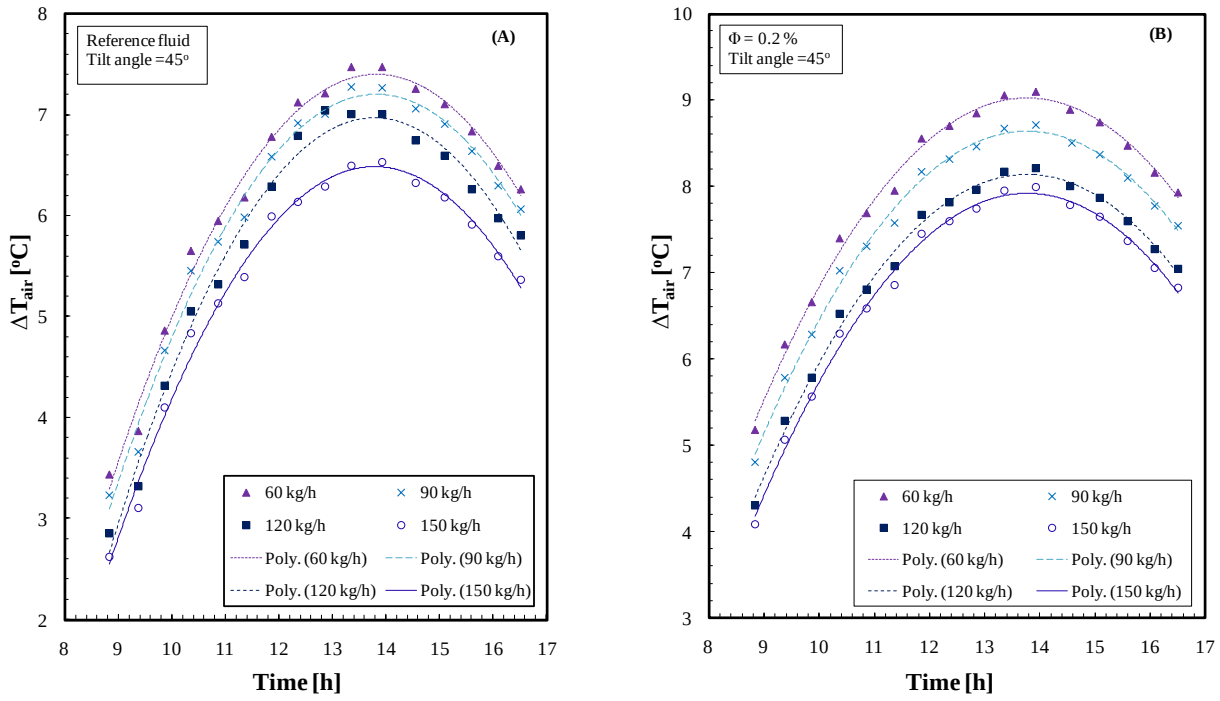

Fig.(20) Airside temperature difference vs time for base water at different mass flow rates

,[A] Reference fluid, **[B]**working fluid with 0.2% nanofluid concentration

Fig. 20 presents the difference in air side temperature with mass flow rates. Low mass flow rate gives the highest difference in air temperature, because it is directly proportional to the water temperature difference. On the other hand, the nanofluid enhances the difference in air temperature. This difference reaches to 9°C at 0.2% of nanofluid concentration, while the difference is 7.5°C for reference fluid at 1:30 PM and 60 kg/h flow rate.

7. Conclusion:

This paper presents an experimental study to investigate the effects of collector tilt angle, nano fluid concentrations and mass flow rates on the performance characteristics of ETHPSC and air heat gain. From the results can be concluded that:

1. According to Cairo latitude the optimum tilt angle is 45°, by tilt angle of 45° the intensity of solar radiation reaches to 940 W/m^2 at 1:30 PM. The air temperature increases by 7.2°C using distilled water as working fluid through 45° tilt angle and at 1:30 PM.
2. By using distilled water, the thermal efficiency at 45° tilt angle is increased by 6.4%, 12.4% and 24.5% compared with the thermal efficiencies at 35°, 25° and 15°; respectively at 1:30 PM.

3. The thermal optical efficiency $F_R(\tau\alpha)$ has high values at 45^o tilt angle, which are 0.477, 0.544, 0.652 and 0.686 at flow rates of 60 kg/h, 90 kg/h, 120 kg/h and 150 kg/h; respectively.
4. The difference in the working fluid temperature promotes by nanofluid addition. The temperature difference of working fluid is highest at a concentration of 0.2%, which is 16% higher than the reference fluid (0%) at 1:30 PM and a flow rate of 90 kg/h.
5. Useful heat gain of ETHPSC increases with increasing nanofluid concentrations. At flow rate of 90 kg/h and at 1:30 PM, the useful heat gain is higher than the reference fluid by 16.5%, 10.8% and 7.3% at concentrations of 0.2%, 0.15% and 0.1%; respectively.
6. With high values of nanofluid concentrations the air temperature difference enhances. The air temperature difference is increased than the reference fluid by about 16.4%, 10.3% and 7.8% at nanofluid concentrations of 0.2%, 0.15% and 0.1%; respectively, at 1:30 PM and a flow rate of 90 kg/h .
7. The thermal optical efficiency is increased by increasing the mass flow rate. By 0.2% nanofluid concentration, the thermal optical efficiency are higher than the reference fluid by about 10.2%, 8.8%, 18% and 23% at mass flow rates of 150 kg/h, 120 kg/h, 90 kg/h and 60 kg/h; respectively.
8. The air temperature difference is higher at low mass flow rate. At 60 kg/h flow rate, the differences in air temperature are 9^oC and 7.5^oC for 0.2% of nanofluid concentration and for reference fluid; respectively.

8. References:

[1] *Sharafeldin M. A.*, 'Evacuated tube solar collector performance using CeO_2 / water nano fluid', Journal of Cleaner Production, vol. 185, pp. 2–11, 2018.

[2] *Sharafeldin M. A.*, 'Efficency of evacuated tube solar collector using WO3/ water nanofluid', Renewable energy, vol. 134, pp. 453–460, 2019.

[3] *Ayompe L. M. and Duffy A.*, 'Thermal performance analysis of a solar water heating system with heat pipe evacuated tube collector using data from a field trial', Solar energy, vol. 90, pp. 17–28, 2013.

[4] *Hyeongmin K., Jinhyun K., Honghyun C.*, 'Experimental study on performance improvement of U-tube solar collector depending on nanoparticle size and concentration of Al_2O_3 nanofluid' Energy, vol.118, pp.1304-1312, 2017.

[5] *Hussain H. A., Q. Jawad, K. F. S.*, ' experimental analysis on thermal efficiency of evacuated tube solar collector by using nanofluids' Solar energy, vol. 4, pp. 19–28, 2015.

[6] *Javad G., Sidik N. A. C.* 'An experimental investigation on the effect of Al2O3/distilled water nanofluid on the energy efficiency of evacuated tube solar collector' International Journal of Heat and Mass Transfer, vol. 108, pp. 972-987, 2015.

[7] *Pise G. A., Salve S. S., Pise A. T., and Pise A. A.*, 'Investigation of Solar Heat Pipe Collector Using Nanofluid and', Energy Procedia, vol. 90, pp. 481–491, 2016.

[8] *Al-Mashat, S.M.S., Hasan, A.A.*, 'Evaluation of convective heat transfer and natural circulation in an evacuated tube solar collector ', Journal of thermal engineering, vol. 19, pp. 613-628, 2013.

[9] *Putra N., Kristian M. R., David R., Haliansyah K., and Ariantara B.*, 'Thermal performance of evacuated tube heat pipe solar collector', American institute of physics, vol. 050004, pp. 1-9, 2016.

[10] *Kang W., Yunchan S., Honghyun C.*, 'Experimental investigation on the heat transfer performance of evacuated tube solar collector using CuO nanofluid and water', Journal of Mechanical Science and Technology, vol. 33, pp 1477–1485, 2019.

[11] *Daghigh R., Shafieian A.*, 'Theoretical and experimental analysis of thermal performance of a solar water heating system with evacuated tube heat pipe collector', Applied Thermal Engineering, vol. 103, pp. 1219–1227, 2016.

[12] *Kaya H., Arslan K., Eltugral N.*, 'Experimental investigation of thermal performance of an evacuated U-Tube solar collector with ZnO/Etylene glycol-pure water nanofluids' Renewable Energy , vol. 122, pp. 329-338, 2018.

[13] *Kiran B. N., Bhowmik M., Muthukumar P.*, 'Experimental investigation and numerical modelling on the performance assessments of evacuated U-Tube solar collector systems', Renewable Energy, vol. 134, pp. 1344-1361, 2019.

[14] *Mustafa A. E*, 'Effects of different working fluid use on the energy and energy performance for evacuated tube solar collector with thermosyphon heat pipe', Renewable Energy, vol. 96, pp. 244-256, 2016.

[15] *Jafarkazemi F., Branch S. T., Ahmadifard E.*, 'Energy and exergy efficiency of heat pipe evacuated tube solar collectors', thermal scince, vol. 20, pp. 327-335, 2016.

[16] *Olcha A., Cholewa T., Dopieralska-Howoruszko K.*, 'Experimental Investigations of Energy and Exergy Efficiencies of an Evacuated Tube Solar Collector', Proceeding, doi:10.3390/proceedings2019016002.

[17] *Iranmanesh S., Ong H. C., Ang B. C., Sadeghinezhad E., Esmaeilzadeh A., Mehrali M.*, 'Thermal performance enhancement of an evacuated tube solar collector using graphene nanoplatelets nanofluid', Journal of Cleaner Production, vol. 162, pp. 121-129, 2017.

[18] *ASHRAE Standard 93* 'Method of testing to determine the thermal of solar collector', Atlanta, GA, USA. 2003

[19] *ASHRAE Handbook of Fundamentals*, SI Edition, Chapters 5 and 14. Atlanta: ASHRAE. 2013.

[20] *Holman, J.P.* Experimental Method for Engineers, 8th Ed., 62–65. New York: McGraw-Hill Book Company. *2001*.

[21] *Fabio S.* 'Analysis of a flat-plate solar collector', Project Report, MVK160, Heat and Mass Transport, Lund, Sweden; 2008.

[22] *Shepherd DW*. 'Energy studies', 2nd Ed., London, UK: Imperial College; 2003.